Electric Field Gradients Around Point Defects in Metals *

Alfred Seeger [a, b], Jörg Ehmann [a], and Manfred Fähnle [a]

[a] Max-Planck-Institut für Metallforschung, Institut für Physik, Heisenbergstraße 1, D-70569 Stuttgart
[b] Universität Stuttgart, Institut für Theoretische und Angewandte Physik, Pfaffenwaldring 57, D-70569 Stuttgart

Z. Naturforsch. **51a**, 489–505 (1996); received February 3, 1996

The splittings of nuclear energy levels caused by the electric field gradients acting on the quadrupole moments of nuclei in the neighbourhood of atomic defects in cubic metals may serve as "fingerprints" providing us with a unique characterization of these defects. In favourable cases the NQDOR technique (nuclear quadrupole double resonance) permits sensitive measurements of these splittings with good resolution. The present paper outlines the status of the ab-initio calculation of electric field gradients with emphasis on the theoretical basis (density functional theory with local density approximation) and on the techniques required for handling the specific problems associated with defects. Recent work by the supercell approach on atomic defects in Al and Cu, making use either of the full-potential linearized augmented-plane-wave method or of the ab-initio pseudopotential method, are reported and compared with experiments. The excellent agreement between experiment and theory for the field gradients acting on the nearest-neighbour nuclei of monovacancies in Al demonstrates the reliability and the potential of the theory.

Key words: Electric field gradients; Core contributions; Ab-initio electron theory; Nuclear quadrupole double resonance; Atomic defects in Al and Cu.

Introduction

Quadrupolar splitting of the energy levels of nuclei possessing electric quadrupole moments Q occurs only if the traceless symmetric rank-two tensor of the gradient of the electric field, V, does not vanish at the nuclear sites. This tensor is zero by symmetry if the nuclear sites have cubic (or isotropic) point symmetry. As a consequence, in perfect crystals with face-centered cubic (A1) or body-centered cubic (A2) structure, but also in perfect NaCl-type (B1) or CsCl-type (B2) crystals as well as others, there will be no quadrupolar level splittings, irrespective of the magnitude of Q. Any perturbation of the perfect lattice structure, however, destroys the cubic point symmetry at the lattice sites in its immediate neighbourhood. Provided the nuclei carry a sufficiently large electric quadrupole moment, this gives us the possibility – at least in principle – to study such perturbations, in the following called "defects", by nuclear magnetic resonance (NMR) measurements. This was recognized and worked out rather fully quite early in the development of NMR, as may be seen, e.g., from the review by Bloembergen [1]. At that time the only experimental technique available was to observe, by NMR in large applied magnetic fields, the transitions between the quadrupolar-split Zeeman levels of the nuclei. It was realized [1] that because of its low sensitivity this technique required defect concentrations ($> 10^{-3}$) that cannot normally be achieved with *intrinsic* atomic defects such as vacancies and self-interstitials. Another disadvantage of the "classical" method of studying the quadrupolar effects due to defects in cubic crystals by measuring the splitting of the Zeeman NMR levels is that well resolved transitions are obtained only if the electric field gradients (efg) at the nuclei are fairly large. This condition is only rarely satisfied for intrinsic atomic defects in metals. The early experimental work on quadrupolar effects due to crystal defects concentrated therefore entirely on dislocations (introduced by extensive plastic deformation) and on foreign atoms on regular lattice sites (in the case of metals: dilute alloys). In these cases the fraction of the nculei experiencing sufficiently large efg could be made large enough to permit quantitative investigations.

The situation began to change when Redfield [2] developed the **n**uclear **q**uadrupole **do**uble **r**esonance

* Presented at the XIIIth International Symposium on Nuclear Quadrupole Interactions, Providence, Rhode Island, USA, July 23–28, 1995.

Reprint requests to Prof. Dr. A. Seeger.

0932-0784 / 96 / 0500-0489 $ 06.00 © – Verlag der Zeitschrift für Naturforschung, D-72072 Tübingen

(NQDOR) technique which, when applicable, gave not only much higher sensitivity than standard NMR absorption measurements but in addition improved the resolution substantially, thus allowing level splittings to be detected down to the so-called dipolar line-width (typically a few 10^4 Hz). The NQDOR technique combines signal detection by conventional NMR in a high magnetic field with quadrupole resonance (NQR) in zero magnetic field. It has been described in detail at the XIIth International Symposium on Nuclear Quadrupole Resonance [3], with special emphasis on the NQDOR equipment built up at the Max-Planck-Institut für Metallforschung in Stuttgart during the last decade [3, 4].

From the point of view of metal physics, the NQDOR technique has the weakness that it is applicable only to a limited number of metals (for details see [3]). So far NQDOR measurements have been reported on the face-centered cubic (fcc) metals aluminium and copper. For many years the experiments concentrated on *dilute alloys* of Cu [3, 5] and Al [6–11]. The first reports on NQDOR experiments involving *intrinsic atomic defects* in metals were those on electron-irradiated Al by Minier, Andreani, and Minier [12] in 1978 and on electron-irradiated Cu by Minier, Minier, and Andreani [13] in 1980. More recently, the NQDOR work on intrinsic atomic defects in Cu and Al has been considerably extended by the Stuttgart group. Examples are the study of Cu that had been electron-irradiated at 90 K [3, 14] or at 20 K [15], of Al electron-irradiated at 90 K [15], of dilute CuBe alloys that were electron-irradiated at 90 K [3], of Cu cold-worked at 77 K or proton-irradiated at 140 K [3, 14], of Cu rapidly quenched either from the melt [16] or from the solid-state near the melting point [15], and of Al quenched from the solid-state [15].

The efg generated by atomic defects in metals may serve as *fingerprints* that allow us to identify a given type of defect under quite different experimental conditions. In contrast to the earlier survey [3], which emphasized the experimental technique and contained only a brief overview of the calculation of efg introduced by point defects in cubic metals, the present review concentrates on ab-initio computations of these quantities. The ultimate goal of the program going on at the Max-Planck-Institut für Metallforschung in Stuttgart is to assign, with the help of theory, the observed quadrupolar transition frequencies to well-defined defects. In the case of intrinsic defects this requires an "interactive" approach involving computations as well as a wide range of experiments.

The computations necessitate various approximations. Among them, the most difficult to control is the so-called local-density approximation (LDA) within the framework of the density functional theory (see Sect. 1.2). The comparison between computed and experimentally determined efg allows us to test the validity and reliability of the theory. In such a comparison two major problems may arise.

(i) Whereas the theory provides us with numerical values of the *electric field gradients* at the nuclei, the experiments give us transition frequencies. Relating these quantities to each other requires knowledge of the *electric quadrupole moments* of the nuclei and of the *asymmetry* η of the efg tensor.

(ii) A critical test of the theoretical predictions is possible only if we can be sure that computations and measurements pertain to the same defects. While this present rarely a serious problem for dilute alloys, the demonstration that the requirement is satisfied is much more difficult for *intrinsic* point defects. The reason is that in *irradiation* or *cold-working* experiments always more than one type of defect is generated. Even under the somewhat simpler condition of metals that have been rapidly quenched from high temperatures, we have to allow for the possibility that a substantial fraction of the quenched-in vacancies is present not as monovacancies but as divacancies or larger agglomerates.

The accuracy with which the *nuclear quadrupole moment* Q is known may vary substantially from nuclide to nuclide. Examples are provided by the nuclides with which the present paper is concerned, viz. ^{27}Al, ^{63}Cu, and ^{65}Cu.

According to Sundholm and Olsen [17] the quadrupole moment of ^{27}Al is

$$Q(^{27}\mathrm{Al}) = (140.3 \pm 1.0) \cdot 10^{-31}\ \mathrm{m}^2 . \qquad (1)$$

The authors arrived at this value by combining the measured nuclear quadrupole coupling constant, $eV_{zz}Q/h$ (e = elementary electric charge, h = Planck's constant), with the efg at the nucleus of Al ($3s^2$, $3p$; $^2P_{3/2}$) atoms as obtained by ab-initio multiconfigurational Hartree-Fock calculations. The uncertainty in (1) is claimed to be less than 1%, i.e. smaller than the computational errors in the calculation of the field

gradients reported in this paper. This means that for the comparison of NQDOR experiments on Al with the theory the uncertainty of Q is negligible.

The situation is different for Cu. While the ratio of the quadrupole moments of the stable Cu isotopes,

$$Q(^{63}\mathrm{Cu})/Q(^{65}\mathrm{Cu}) = 1.079\,, \tag{2}$$

is known with high accuracy from the NQDOR work of Minier and Minier [5], the absolute Q values are much less certain. The value recommended by Pyykkö and Li [18], which comes from the X-ray measurement of the hyperfine structure of mesonic Cu atoms,

$$Q(^{63}\mathrm{Cu}) = -(220 \pm 15)\cdot 10^{-31}\ \mathrm{m}^2\,, \tag{3}$$

has an uncertainty of about 7%. This has to be taken into account in the comparison between experiment and theory.

For a given defect, the *asymmetries* at the various sites, defined as

$$\eta := (V_{xx} - V_{yy})/V_{zz}\,, \tag{4}$$

where the principal components V_{ii} of the efg tensor are chosen in such a way that

$$|V_{zz}| \geq |V_{yy}| \geq |V_{xx}|\,, \tag{5}$$

should come out of the computations. With regard to the comparison theory – experiment the situation is again quite different for Al and Cu. In NQDOR experiments on ^{27}Al (spin 5/2) η may be deduced from the ratios ν_2/ν_1 of the transition frequencies of the $|m| = 3/2 \leftrightarrow |m| = 5/2$ and the $|m| = 1/2 \leftrightarrow |m| = 3/2$ transitions. Since the nuclides of natural Cu, ^{65}Cu and ^{63}Cu, have both spin 3/2, in zero magnetic field they give rise to one transition ($1/2 \leftrightarrow 3/2$) only, with frequency [19]

$$\nu_q = \frac{eQ|V_{zz}|}{2h}\sqrt{1+\frac{\eta^2}{3}}\,. \tag{6}$$

From (6) the separate determination of $|V_{zz}|$ and η is not possible. The separation may become possible by means of the nutation technique [20]; however, so far this technique has not been applied to NQDOR.

The general theory involved in the calculation of efg in solids is treated in Sect. 1. Subsect. 1.2 gives an outline of ab-initio electron theory with special emphasis on the approximations required for practical computations. Subsect. 1.3 focuses on the computation of the efg tensor with special regard to the influence of the core electrons on the efg. Sect. 2. reports the results of recent calculations of the efg generated by intrinsic atomic defects or substitutional foreign atoms in Al and Cu. The results will be compared with the numerical values obtained by other theoretical approaches on the one hand, and with NQDOR measurements on the other hand. Finally, Sect. 3. summarizes the conclusions that may be drawn from the present work.

1. Ab-initio Calculation of Electric Field Gradients Introduced by Atomic Defects

1.1 Definition of the efg Tensor

The traceless symmetric tensor of the electric field gradients (efg) at a nucleus, $V = (V_{ij})$, is defined as

$$V_{ij} = \left.\frac{\partial^2 \Phi}{\partial x_i \partial x_j}\right|_{\text{nucleus}} - \frac{1}{3}\delta_{ij}\Delta\Phi\Big|_{\text{nucleus}}\,, \tag{7}$$

where

$$\Phi(\boldsymbol{r}) = \int \frac{\varrho(\boldsymbol{r}')}{|\boldsymbol{r}-\boldsymbol{r}'|}\,\mathrm{d}\boldsymbol{r}' \tag{8}$$

is the electrostatic potential and $\varrho(\boldsymbol{r})$ the total ground-state charge density of the system. The subscript "nucleus" indicates that all derivatives have to be taken at the position of the nucleus considered, which in the following will be taken as the origin of our coordinate system. Inserting (8) into (7) gives us

$$V_{ij} = \int \varrho(\boldsymbol{r})\left(\frac{3x_i x_j}{r^5} - \frac{\delta_{ij}}{r^3}\right)\mathrm{d}\boldsymbol{r}\,. \tag{9}$$

According the (9) the part of $\varrho(\boldsymbol{r})$ that has *spherical* symmetry around the nucleus does not contribute to V. Because of the singular behaviour of the expression in parenthesis at the origin, the *non-spherical* contribution to the total charge density of the system must be determined with high accuracy in order to calculate the efg tensor reliably. For solids, the appropriate tool to do this is ab-initio electron theory. Since the NQDOR experiments are carried out at low temperatures (typically at about 2 K) we may confine ourselves to ground states.

1.2 Ab-initio Electron Theory

The full description of the ground state of a solid requires the knowledge of its many-body wavefunction, which depends on the coordinates of all nuclei and electrons. In practice it is impossible to solve the

many-body Schrödinger equation of a solid without approximations. As a first simplifying approximation use is made of the Born-Oppenheimer approximation [21, 22]. It rests on the fact that the electron mass is much smaller than the nuclear masses. Therefore the electrons are able to follow the motions of the nuclei virtually instantaneously. As a consequence, the positions of the nuclei, $\boldsymbol{R}_\alpha$, may be considered as classical parameters. Then the electrons obey a many-body Schrödinger equation that depends on these parameters. The Born-Oppenheimer approximation, also known as *adiabatic approximation*, is well established in molecular or atomic physics as well as in solid state physics. In the present context its use is not critical [22].

The most important tool to calculate the ground-state properties of an extended *electronic* system such as that of a solid is the *density-functional theory* (DFT) of Hohenberg and Kohn [23]. It is based on the fact that the ground-state properties (e.g., total energy, efg) of a system of interacting electrons in an external potential (usually the Coulomb potential of the nuclei at the positions $\boldsymbol{R}_\alpha$) are completely determined by the ground-state electronic density, $n_e(\boldsymbol{r})$. The total energy of the system, E, and all other ground-state properties are functionals of $n_e(\boldsymbol{r})$. The correct ground-state density is the density that minimizes the total-energy functional, $E = E[n_e]$. Kohn and Sham [24] showed that it can be obtained by solving self-consistently a single-particle Schrödinger equation containing an effective potential. This equation is called Kohn-Sham equation; the solutions are the so-called Kohn-Sham orbitals.

Unfortunately, the preceding recipe of how to obtain the ground-state electronic density has the character of a *proof of existence*, since the true form of $E[n_e]$ is only incompletely known. We may – still rigorously – subdivide $E[n_e]$ according to

$$E[n_e] = T_{el}[n_e] + E_H[n_e] + E_{ext}[n_e] + E_{xc}[n_e] \qquad (10)$$

into the kinetic energy functional of noninteracting particles, $T_{el}[n_e]$, with the same density n_e as the interacting electrons, the so-called Hartree functional $E_H[n_e]$ of the Coulomb interaction between the electrons, the functional $E_{ext}[n_e]$ of the Coulomb interaction between the electrons and the nuclei, and the exchange-correlation (xc) functional $E_{xc}[n_e]$. It is this last term that remains unknown. Its exact form, if known, could be very complicated. The usefulness of DFT depends therefore critically on whether we can find (a better expression may be "guess") a sufficiently accurate approximate expression for $E_{xc}[n_e]$. Within the framework of the DFT the most frequently used approach to the exchange-correlation problem is the so-called *local-density approximation* (LDA) [24]. In the LDA, the xc functional is approximated by

$$E_{xc}[n_e] = \int n_e(\boldsymbol{r})\,\varepsilon_{xc}(n_e(\boldsymbol{r}))\,\mathrm{d}\boldsymbol{r}\,, \qquad (11)$$

where $\varepsilon_{xc}(n_e)$ is the xc density per electron of a homogeneous electron gas. $\varepsilon_{xc}(n_e)$ can be determined with the help of more elaborate many-body calculations (see, e.g., [25]).

As already mentioned in the Introduction, among the approximations employed in the present approach to the ab-initio calculation of ground-state physical properties of condensed matter LDA is the one that is most difficult to control. By way of example this may be seen by comparing the lattice constants as calculated ab-initio using LDA with the measured ones. Invariably they come out too small, in Li and Na by 4%, in Cu by 2%, and in Al by 1%.

The literature contains various attempts to improve on the local density approximation (e.g., the generalized gradient approximation (GGA) [26]), but since their domains of usefulness have not yet been clearly established (see e.g., [27]), they will not be used in the present paper. A point clearly in favour of the GGA is that for Al and Cu the lattice constants calculated ab-initio are in better agreement with the measured ones than those obtained from LDA. If the same lattice constants are used in LDA and GGA computations, the results for the efg differ only slightly, however.

With the help of DFT and LDA the original many-body problem has been reduced, though only approximately so, to the solution of a single-particle Schrödinger equation,

$$\left(-\frac{\hbar^2}{2m_e}\Delta + \Phi_{eff}(\boldsymbol{r})\right)\Psi_i(\boldsymbol{r}) = \varepsilon_i\,\Psi_i(\boldsymbol{r})\,, \qquad (i = 1, 2, \ldots, N_e) \qquad (12)$$

(m_e = electron mass) for all N_e electrons of the system, containing an effectice potential, $\Phi_{eff}(\boldsymbol{r})$, that is given by

$$\Phi_{eff}(\boldsymbol{r}) = \Phi_{ext}(\boldsymbol{r}) + \Phi_H(\boldsymbol{r}) + \Phi_{xc}(\boldsymbol{r})\,. \qquad (13)$$

In (13) $\Phi_{ext}(\boldsymbol{r})$ denotes the Coulomb potential of the nuclei,

$$\Phi_H(\boldsymbol{r}) = e^2 \int \frac{n_e(\boldsymbol{r}')}{|\boldsymbol{r} - \boldsymbol{r}'|}\,\mathrm{d}\boldsymbol{r}' \qquad (14)$$

the so-called Hartree potential, and

$$\Phi_{xc}(\boldsymbol{r}) = \frac{\delta E_{xc}[n_e]}{\delta n_e} \tag{15}$$

the exchange-correlation potential. Φ_{xc} accounts for classical (e.g., Coulomb correlations between the electrons) as well as quantum-mechanical (e.g., Pauli's exclusion principle) many-body effects, which cannot be covered by a single-particle Schrödinger equation. In LDA it reads

$$\Phi_{xc}(\boldsymbol{r}) = \frac{\mathrm{d}}{\mathrm{d}n_e}\left[n_e(\boldsymbol{r})\,\varepsilon_{xc}(n_e(\boldsymbol{r}))\right]. \tag{16}$$

Since the Kohn-Sham orbitals $\Psi_i(\boldsymbol{r})$ are normalized to one, $\int |\Psi_i(\boldsymbol{r})|^2\,\mathrm{d}\boldsymbol{r} = 1$, the electronic density of the system is obtained in the usual way through

$$n_e(\boldsymbol{r}) = \sum_{i=1}^{N_e} |\Psi_i(\boldsymbol{r})|^2 . \tag{17}$$

The equations (12), (13), and (17) are called Kohn-Sham equations. They may be solved self-consistently to give us single-particle energies ε_i and Kohn-Sham orbitals $\Psi_i(\boldsymbol{r})$ for all N_e electrons of the system as well as the electronic density $n_e(\boldsymbol{r})$ by starting with a suitably chosen effective potential $\Phi_{eff}(\boldsymbol{r})$, feeding the electronic density $n_e(\boldsymbol{r})$ derived from it back into (14) and (16) to obtain an improved effective potential (13), and repeating this procedure until $n_e(\boldsymbol{r})$ no longer changes significantly. The practical side of this procedure will be briefly discussed below.

According to Bloch's theorem [28], in periodic structures the Kohn-Sham orbitals are Bloch waves. This has the practical consequence that if suffices to solve the Kohn-Sham equation (12) on a grid of sampling points in the first Brillouin zone of the structure. However, the perturbation of the perfect lattice structure by an atomic defect destroys the periodicity of the crystal. Hence Bloch's theorem is no longer valid. One way of dealing with this problem is to use the so-called supercell method.

The *supercell method* considers an array of periodically arranged atomic defects and applies Bloch's theorem to this periodicity rather than to that of the perfect crystal. The crystal is thus made up of "supercells", each of which contains one defect. If, as in the present case, we wish to study the properties of isolated defects, the supercell size should be so large that defect-defect interactions are negligible. (This is the case if a further increase of the supercell size leaves the results unchanged.) In practice, this can only rarely be achieved. One has therefore to pay attention to "finite-size" effects and correct for them if necessary and possible.

The methods for obtaining numerical solutions of the Kohn-Sham equations differ in the choice of the basis functions into which the Kohn-Sham orbitals of the valence electrons are expanded. In the work to be reported in Sect. 2.2 the full-potential linearized augmented-plane-wave (FLAPW) method [29, 30] and the plane-wave pseudopotential method (see, e.g., [31]) have been used.

In the FLAPW method the wavefunctions of the valence electrons are expanded in plane waves which in the vicinity of the nuclei are replaced ("augmented") by atomic wavefunctions. The atomic wavefunctions are the solutions of the spherically averaged Kohn-Sham equation (12) for a suitably chosen energy. The augmentation of the plane waves is necessary because the Kohn-Sham orbitals vary rapidly near the nuclei and are therefore in this region not suited for an expansion in plane waves.

The basic idea of the pseudopotential method is to find a transformation which eliminates both the closed-shell core states and the rapid variations in the valence states in the core region out of the formalism. Its roots go back to Hellmann and Kassatotschkin [32, 33]. In their "combined approximation procedure" they treated the core electrons by the Thomas-Fermi method and the valence electrons according to a Schrödinger equation containing an additional potential which describes the interaction of the valence electrons with the core electrons. The early work on "pseudopotentials" was reviewed by Gombás [34]. The objects called pseudopotentials in [34] are potential-like terms in the Schrödinger equation that were designed to account for exchange and correlation interactions as well as for Pauli's exclusion principle but which did not replace the Coulomb potentials of the nuclei. In 1952 Fues and Statz showed [35] that it is possible to replace the Coulomb potential of the ion cores (nuclei plus core electrons) by an "ersatz potential" without changing the wavefunctions and energies of the valence electrons significantly. Rather less descriptively, such "ersatz potentials" were later called model potentials or pseudopotentials [36].

The modern ab-initio pseudopotential [37] methods replace the Coulomb potential of each nucleus inside a radius r_c by a "pseudopotential" that is constructed ab-initio in such a way that it reproduces the scatter-

ing properties of the ion cores. The spatial variation of the pseudopotential may be made week enough to be handled by a plane-wave expansion of the "pseudo-wavefunctions" (= solutions of the transformed Schrödinger equation). The price to pay for this simplification is that the valence-electron density calculated from the pseudo-wavefunctions by means of (17) is correct only in the interstitial regions, i.e. the regions outside the spheres of radius r_c around the nuclei. However, the contribution of the valence electrons to the efg at the nuclei (in the following simply called "valence contribution") can be obtained correctly only if the non-spherical part of the valence-electron density is known with sufficient accuracy. For the present application of the ab-initio pseudopotential method it is therefore essential that the true, aspherical valence-electron wavefunction can be reconstructed from the pseudo-wavefunction [38, 39].

The reconstruction proceeds as follows. The Kohn-Sham equations are solved self-consistently inside a sphere of radius r_{rec} (chosen slightly larger than r_c) using the electrostatic potential due to the nucleus and its core electrons as external potential Φ_{ext}. The aspherical boundary conditions at $r = r_{rec}$ are taken from the pseudopotential calculation. As a matter of principle, the accuracy of the valence-electron density obtained in this way and of the efg derived from it is limited by the over-all accuracy of the pseudopotential method. Since the reconstruction technique may introduce small additional inaccuracies, the efg obtainable by the ab-initio pseudopotential method will clearly be less accurate than those computed by the FLAPW method. This drawback has to be weighted against the fact that the plane-wave pseudopotential method requires much less computational effort than the FLAPW method, especially for simple metals such as Al. An example will be given in Sect. 2.2.1, where the pseudopotential method has enabled us to treat a large supercell containing as many as 124 Al atoms.

In problems dealing with crystals containing defects, the strength of both the FLAPW method and the plane-wave pseudopotential method is that they permit to calculate ab-initio the forces acting on the nuclei and thus to allow fully for the so-called lattice relaxation, i.e. for the fact that in the neighbourhood of an atomic defect the nuclei are displaced from their regular lattice sites. The relaxed positions of the nuclei are determined by moving them under the influence of the forces until all of them have reached positions of zero force. By a systematic procedure this can be achieved with an acceptable numerical effort. In both methods the formula for the atomic forces simplify when it is assumed that the electronic density has been determined self-consistently for the given basis set. In this case the plane-wave pseudopotential method yields just the Hellmann-Feynman force [40], which is the physical electrostatic force on the nuclei. The FLAPW method, however, requires correction terms arising from the localized parts of the basis functions of the (in practice) incomplete basis set. In the present paper the force formula of Soler and Williams [41] is employed. This formula, which was originally developed for the APW method of Soler and Williams [41], has recently been shown [42] to be applicable to the FLAPW basis set, too. A general approach to the computation of ab-initio forces without regarding to a special basis set is given in [43].

The high-accuracy determination of the lattice relaxation is essential for the reliable computation of the efg around atomic defects in crystals since these depend sensitively on the positions of the nuclei (see Sect. 2). In this respect the supercell method is clearly superior to the alternatives that have been in the literature, viz. the *Green's function method* [44] and *real-space cluster calculations*.

The *Green's function (GF) method*, which considers the atomic defect as a localized perturbation of an otherwise perfect crystal, was combined with the Korringa-Kohn-Rostoker (KKR) method [45, 46] by Dederichs et al. [47] in a full-potential version. In contrast to the two methods used in the present work, in this KKR-GF method the lattice relaxation around an atomic defect cannot be calculated by moving the atoms until the computed forces on them vanish. The main reason for this is that the KKR-GF method employs the Green's function of the ideal crystal rather than that of the perturbed crystal. Hence in the computation all atoms outside the defect must be placed on regular lattice sites. An approximate way to take the lattice relaxation into account is to compute the forces acting on the atoms at regular lattice sites and determine their displacements under these forces from lattice statics, making use of the Born-von-Karman coupling parameters as obtained from the phonon spectra of the ideal crystal. Since these parameters do not allow for defect-induced changes, this procedure can give reliable results only if the lattice relaxations are small, as may be the case around monovacancies or substitutional foreign atoms. The method is definitely less suitable for self-interstitials,

e.g., ⟨100⟩ dumb-bells in fcc metals, since here some atoms are located far from regular sites. This difficulty may be circumvented, at least in principle, by increasing the size of the defect, i.e. by considering the original atomic defect together with a cluster of a few surrounding shells of neighbouring atoms as "defect", Inside the "defect" the relaxation can be carried out using the computed interatomic forces. However, the required increase in size of the defect would entail a large increase in computation time. For the time being, this makes this approach to the self-interstitial problem rather impractical.

In order to perform *real-space cluster calculations* of efg even for small clusters, several approximations have to be made, some of which may be quite serious. We illustrate this for the real-space linear-muffin-tin-orbital method [48]. Here the most serious approximation in the computation of efg generated by defects is the so-called atomic-sphere approximation (ASA) [49]. This approximation replaces the Wigner-Seitz cells of the atoms by spheres of equal volume, inside of which the potential is assumed to be spherically symmetric. It is obvious that the ASA may influence the accuracy of the aspherical part of the valence-electron density and thus the computed efg considerably. Furthermore, within the ASA the computation of atomic forces is a serious problem. At present, in the real-space linear-muffin-tin-orbital method the lattice relaxation cannot be taken into account in a satisfactory way. The consequences of this will be illustrated in Sect. 2.2.1.

1.3 Computation of the Electric Field-Gradient Tensor

As outcome of a self-consistent FLAPW calculation or of a pseudopotential calculation with subsequent reconstruction of the true valence wavefunctions the aspherical *valence-electron density*, $n_v(\boldsymbol{r})$, and the positions of the nuclei, $\boldsymbol{R}_\alpha$, are known. In both types of calculation the *core states* have initially been assumed to be spherically symmetric. This allows us, in the computation of the efg, to replace them by point charges and to combine them with the nuclear charges to give us ion charges $e Z_\alpha^{\text{ion}}$ located at $\boldsymbol{R}_\alpha$. The total charge density of the crystal may thus be written as

$$\varrho(\boldsymbol{r}) = e \sum_\alpha Z_\alpha^{\text{ion}} \delta(\boldsymbol{r} - \boldsymbol{R}_\alpha) - e\, n_v(\boldsymbol{r}) . \tag{18}$$

Inserting (18) into (9) gives us the following expression for the sum of the contributions of the ion charges $e Z_\alpha^{\text{ion}}$ (in the following called *lattice contribution*) and of the valence electrons to the tensor of the efg at a nucleus in the origin of the coordinate system ($\boldsymbol{R}_0 = \boldsymbol{0}$):

$$V_{ij}^{\text{val+lat}} = e \sum_\alpha{}' Z_\alpha^{\text{ion}} \left(\frac{3(\boldsymbol{R}_\alpha)_i (\boldsymbol{R}_\alpha)_j}{R_\alpha^5} - \frac{\delta_{ij}}{R_\alpha^3} \right) - e \int n_v(\boldsymbol{r}) \left(\frac{3 x_i x_j}{r^5} - \frac{\delta_{ij}}{r^3} \right) \mathrm{d}\boldsymbol{r} . \tag{19}$$

In (19) the dashed sum goes over all nuclei, at positions $\boldsymbol{R}_\alpha$, except for the nucleus at the origin.[1]

The fact that so far the core charge density of the nucleus at $\boldsymbol{R}_0 = \boldsymbol{0}$ has been treated as spherically symmetric has the consequence that it does *not* contribute to the efg. However, because of the weighting factor $1/r^3$, the efg is highly sensitive to asphericities of the charge density close to the nucleus. This means that even small deviations of the core charge density of the nucleus at $\boldsymbol{R}_0$ from spherical symmetry may contribute strongly to the efg acting on it. Within the framework of first-order perturbation theory this contribution, V_{ij}^{core}, may be estimated by inserting a factor $(1 - \gamma(r))$ into the integrand of (9) [50, 51] and using $\varrho(\boldsymbol{r})$ of (18). To see this, let us consider the electric quadrupole moment Q of the nucleus at $\boldsymbol{R}_0 = \boldsymbol{0}$ as a perturbation

$$\Phi_Q(\boldsymbol{r}) = - e^2 \sqrt{\frac{\pi}{5}} \frac{Q}{r^3} Y_{20}(\hat{\boldsymbol{r}}) \tag{20}$$

acting on the core electrons. ($Y_{20}(\hat{\boldsymbol{r}})$ = the spherical harmonic of angular momentum $l = 2$ and $m = 0$.) This perturbation induces a quadrupole moment $Q_{\text{ind}}(r)$ in the core charge density. From first-order perturbation theory it follows [52] that the induced quadrupole moment is spherically symmetric and proportional to Q. We may therefore write

$$Q_{\text{ind}}(r) =: - \gamma(r) Q . \tag{21}$$

The function $\gamma(r)$ introduced by (21) is called Sternheimer function. In the approximation leading to (21) the total quadrupole moment of the system nucleus plus core electrons at a distance r from the nucleus is given by $Q_{\text{tot}} = (1 - \gamma(r)) Q$. Outside the region of the core charge density the total quadrupole moment and

[1] In the literature a different notation is occasionally used, in which the lattice contribution to the efg is defined as the contributions of all charges outside a sphere of radius $\simeq d/2$ around the nucleus considered, with d = nearest-neighbour distance.

thus $\gamma(r)$ cannot vary. Therefore, for $r > d/2$, $\gamma(r)$ assumes a constant value, γ_∞, known as Sternheimer or antishielding factor. A charge at a distance r from the nucleus not belonging to the system "nucleus plus core electrons" (e.g., due to valence electrons) "sees" the total quadrupole moment $Q_{\text{tot}}(r)$ rather than the nuclear quadrupole moment Q. Thus, if we wish to express the quadrupolar transition frequencies in terms of the nuclear quadrupole moment Q, we have to multiply the external charges – in the present case those of the valence electrons and the ion charges $eZ_\alpha^{\text{ion}}(\alpha \neq 0)$ – by the factor $(1-\gamma(r))$. This gives us for the core contribution to the efg

$$V_{ij}^{\text{core}} = -e\gamma_\infty {\sum_\alpha}' Z_\alpha^{\text{ion}} \left(\frac{3(\boldsymbol{R}_\alpha)_i (\boldsymbol{R}_\alpha)_j}{R_\alpha^5} - \frac{\delta_{ij}}{R_\alpha^3} \right) + e \int n_{\text{v}}(\boldsymbol{r}) \gamma(r) \left(\frac{3x_i x_j}{r^5} - \frac{\delta_{ij}}{r^3} \right) \mathrm{d}\boldsymbol{r} \,. \quad (22)$$

where in the first term we were justified in replacing $\gamma(r)$ by γ_∞ since the ion charges are at distances from the nucleus that are larger than $d/2$. Within the framework of first-order perturbation theory the determination of V_{ij}^{core} may thus be reduced to the computation of $\gamma(r)$.

In combination with the FLAPW method the present paper uses an alternative approach (see [53, 54]) that has the advantage of not being restricted to perturbation theory. It proceeds as follows.

The self-consistent solution of the Kohn-Sham equations by means of the FLAPW method gives us the effective potential Φ_{eff}. In the vicinity of a nucleus (for simplicity assumed to be at $\boldsymbol{R}_0 = \boldsymbol{0}$) it may be expanded in spherical harmonics according to

$$\Phi_{\text{eff}}(\boldsymbol{r}) = \sum_{lm} \Phi_{lm}^{\text{eff}}(r)\, Y_{lm}(\hat{\boldsymbol{r}}) \,. \quad (23)$$

In the self-consistency procedure described so far the core wavefunctions $\Psi_i(\boldsymbol{r})$ were obtained as solutions of the Kohn-Sham equation (12) with spherically averaged effective potential. As a consequence, the resulting core-electron density is up to now spherically symmetric. The asphericity of the effective potential (23), however, leads to a polarization of the core-electron density. This polarization can be computed at the end of the FLAPW calculation by solving the *aspherical* Kohn-Sham equation

$$\left(-\frac{\hbar^2}{2m_{\text{e}}} \Delta + \sum_{lm} \Phi_{lm}^{\text{eff}}(r)\, Y_{lm}(\hat{\boldsymbol{r}}) \right) \Psi_i(\boldsymbol{r}) = \varepsilon_i \Psi_i(\boldsymbol{r}) \quad (24)$$

for the correct wavefunctions $\Psi_i(\boldsymbol{r})$ of all $z = Z_0 - Z_0^{\text{ion}}$ core electrons, where Z_0 is the charge number of the nucleus under consideration. For "true" core states, i.e. core states whose charge density decreases to zero within $d/2$, (24) is an "atomic" problem, with no solid-state boundary conditions to be satisfied. If the core wavefunctions are known, the – now aspherical – core-electron density is given by

$$n_{\text{c}}(\boldsymbol{r}) = \sum_{i=1}^{z} |\Psi_i(\boldsymbol{r})|^2 \,. \quad (25)$$

Inserting $-e\,n_{\text{c}}(\boldsymbol{r})$ into (9) gives us the contribution

$$V_{ij}^{\text{core}} = -e \int n_{\text{c}}(\boldsymbol{r}) \left(\frac{3x_i x_j}{r^5} - \frac{\delta_{ij}}{r^3} \right) \mathrm{d}\boldsymbol{r} \quad (26)$$

of the core electrons to the efg tensor at $\boldsymbol{R}_0 = \boldsymbol{0}$. From (19) and (26) we thus obtain to a good approximation the total efg tensor

$$V_{ij} = V_{ij}^{\text{val+lat}} + V_{ij}^{\text{core}} \,. \quad (27)$$

As described so far the present method is a "one-shot approximation", since the reaction of the valence electrons to the asphericity of the core-electron density has been neglected. It has the advantage over the Sternheimer-function approach that the computation of the aspherical core-electron density, $n_{\text{c}}(\boldsymbol{r})$, may be included in the self-consistency cycle of the FLAPW method without a significant increase in computational time. Exploratory computations indicate that the "one-shot approximation" may give quite accurate results for the core contributions to the efg. It appears that this is due to the fact that the asphericity of the core charge is in general small compared to that of the valence charge density (see Sect. 2.2).

The approach described above for calculating the core contribution to the efg relies on the fact that the aspherical effective potential (13) is known. In the pseudopotential method the correct from of $\Phi_{\text{eff}}(\boldsymbol{r})$ in the vicinity of the nucleus considered is unknown, owing to the introduction of the pseudopotential. Unfortunately, this is still true after the true valence wavefunctions are reconstructed [39], since in the reconstruction program the small asphericity of the potential inside the reconstruction sphere is neglected. This should be a good approximation since the correct aspherical valence-electron density is almost completely determined by the aspherical boundary conditions supplied by the pseudopotential calculation. Of course, if the correct aspherical charge density is known, we may solve Poisson's equation in order to

obtain the correct aspherical effective potential, but this has so far not been implemented in the reconstruction program. Therefore, at present the calculation of the core contribution to the efg in the pseudopotential formalism is not practicable. The use of the Sternheimer function, $\gamma(r)$, is an alternative, but this has so far not been done either.

Recent progress has allowed us to take into account, within the FLAPW method, the influence of the high-lying core states (e.g., of 3s and 3p electrons in Cu) on the efg together with the valence contribution with the help of so-called local orbitals [55, 56] without significant increase in computing time. The results of a local-orbital calculation and of the "one-shot approximation" will be compared in Sects. 2.2.1 and 2.2.2 for two test cases.

2. Electric Field Gradients in FCC Metals

2.1 Crystallographic Classification

NQDOR allows us, under suitable experimental conditions, to detect NQR transitions of nuclei that experience the same efg. In the investigation of atomic defects in crystals a necessary (but by no means sufficient) condition for this is that these nuclei all have the same distance from the defect centres. Nuclei at the same distance are said to lie on the same shell. We number the shells according to increasing distances in the perfect lattice. In the fcc lattice the distances from a fixed lattice site are

$$d = \sqrt{\frac{n}{2}}\, a_0 \,, \tag{28}$$

where a_0 is the edge length of the elementary cube and $n \in \mathbb{N}$. Examples for the numbering of shells according to (28) are a vacant lattice site or a substitutional foreign atom (Fig. 1, left).

If the efg tensors at the nuclei are not required by symmetry to have the same principal components (they are always allowed to differ in the crystallographic orientation of their axes), we introduce subshells. This is illustrated on the right-hand side of Figure 1. Here a so-called ⟨100⟩ dumb-bell [57] has been introduced into an fcc lattice by taking out an atom from its lattice site and inserting two atoms along a ⟨100⟩ axis symmetrically to the vacant site. It is obvious that the efg in shell 2 generated by the introduction of a ⟨100⟩ dumb-bell will depend on whether the nuclear sites lie on the ⟨100⟩ axis through the defect centre, or on the ⟨010⟩ or ⟨001⟩ axes. Thus in this case shell 2 splits into two subshells 2′ and 2″. The number of sites per defect in a given shell or subshell are called the multiplicity of the shell or subshell.

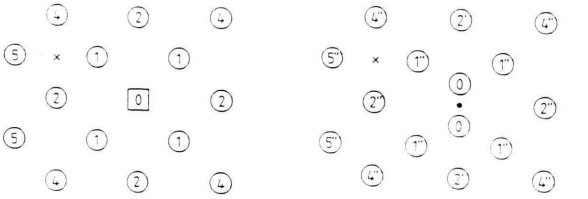

Fig. 1. (001) planes of fcc structure. *Left:* Numbering of shells in the neighbourhood of a vacant lattice site or a substitutional foreign atom (denoted by 0). *Right:* Shells around a ⟨100⟩ dumb-bell (denoted by 0). • denotes the dumb-bell centre.

In the example of Fig. 1 the multiplicity of shell 2 is 6; the multiplicities of subshells 2′ and 2″ are 2 and 4, respectively. For defects with tetragonal point symmetry centered at a lattice point with cubic symmetry the ratio of the multiplicities of the subshells is always 1:2. We distinguish the two subshells by a dash and double dash. Note, however, that in the present case there are shells which do not split, viz. those containing atoms lying on the ⟨111⟩ axes through the defect centre. The shell nearest to the defect that satisfies this condition is shell 6.

The subshells may be characterized further according to whether their efg tensors have two equal principal components or not. The first case corresponds to $\eta = 0$, the second case to $0 < \eta \leq 1$, the limiting case $\eta = 1$ being reached when one of the principal components is zero. (The two others must then differ by a factor -1.) The cases $\eta = 0$ may easily be found by inspection, provided the displacement of the atoms accompanying the introduction of a defect does not reduce the point symmetry (i.e., the point symmetry remains cubic for a vacancy and tetragonal for a ⟨100⟩ dumb-bell even if the "lattice relaxation" (cf. Sect. 2.2) is allowed for).

Table 1 summarizes the preceding discussion for the two configurations of Figure 1. The first line gives the shell number, the second one the radius of the shell (neglecting lattice relaxation) in units of $a_0/\sqrt{2}$. In the third line the multiplicities are listed for vacancies and substitutional foreign atoms. The fourth lines give the multiplicity for ⟨100⟩ dumb-bells. The multiplicities are printed in bold face if $\eta = 0$.

Table 1. Radii of the different shells (neglecting lattice relaxation) around a lattice site in the fcc structures in units of $a_0/\sqrt{2}$ and multiplicities for vacancies and substitutional foreign atoms (cubic point symmetry) as well as for a ⟨100⟩ dumb-bell (tetragonal point symmetry). Bold entries indicate that the asymmetry η of the efg is zero by symmetry.

Shell number	0	1	2	3	4	5	6
Distance from centre	–	1	$\sqrt{2}$	$\sqrt{3}$	2	$\sqrt{5}$	$\sqrt{6}$
Multiplicity							
cubic	–	12	**6**	24	12	24	**8**
tetragonal	**2**	4+8	**2**+4	8+16	4+8	8+16	8

2.2 *Results of Computations*

Compared with the calculation of efg in perfect crystals with non-cubic point symmetry of the nuclear sites (e.g., hexagonal metals [58]), in the computation of efg in the neighbourhood of *defects* two additional problems have to be solved.

(i) The atomic positions around the defects are not given a priori but must be found by computation. This is primarily a problem of computation time, since a large number of equilibrium conditions have to be satisfied simultaneously.

(ii) If problem (i) is tackled by the supercell method, finite-size effects are invariably introduced. They affect the results especially for shells near the supercell surface. This has to be taken into consideration when the theoretical results are compared with experimental data. The finite-size effects may be estimated by performing computations for different supercell sizes and studying their convergence as a function of the cell size.

In the following subsections we report on calculations of atomic positions and efg in the neighbourhood of atomic defects in Al and Cu. The supercell calculations carried out at Stuttgart using either the FLAPW or the pseudopotential method will serve to illustrate the general principles outlined in Sect. 1 and will allow us to perform a preliminary comparison with experimental data. Reference will also be made to the calculation by other authors based on the real-space cluster method [59] or the GF-KKR approach [60].

2.2.1 Results on Al

The supercell calculations on defects in Al to be reported in what follows have all been performed for the ab-initio lattice constant. The efg in the neighbourhood of a monovacancy and the quadrupolar transition frequencies associated with them have been calculated using a supercell size of 124 atoms and the plane-wave pseudopotential method. For this supercell size the atoms of shell 7 lie on the surface of the supercell, i.e. halfway between two monovacancies. We may thus relax the atomic positions in the first six shells, but have to keep in mind that the relaxations of the atoms close to the surface (say, those in shells 5 and 6) will certainly be affected by the finite size of the supercell.

Table 2 gives the results of the positions of the atoms in the neighbourhood of a monovacancy up to shell 4. (The relaxation of the atoms in shell 5 has been neglected, since the forces acting on them are very small.) Using these atomic positions the quadrupolar transition frequencies ν_2 and ν_1 of the first five shells surrounding a monovacancy were computed neglecting the core contribution to the efg. The results are shown in Fig. 2 as square symbols.

In order to test the sensitivity of the computed transition frequencies to small changes of the atomic positions, the computation was repeated with the atoms of shell 4 radially displaced from their relaxed positions by $4 \cdot 10^{-3} a_0$ (circles in Figure 2). The comparison between the two computations demonstrates that the efg may depend very sensitively on the lattice relaxation. It is therefore not straightforward to obtain accurate efg for higher shells.

Figure 3 shows the theoretical values for the transition frequencies ν_2 using the relaxed positions of Table 2 together with the experimental values obtained after low-temperature electron irradiation [12, 15], quenching from high temperatures [15], or cold-work [15]. The assignment of the experimentally observed frequencies to distinct shells is that of Konzelmann et al. [15]. Compared to this, in the assignment suggested by Minier et al. the frequencies of shell two and four are interchanged. Experimental [15] and theoretical values for the asymmetry η, are given in Table 3.

Table 2. Positions of the nuclei around a monovacancy in Al in units of a_0 as computed with a 124-atom supercell and the plane-wave pseudopotential method.

Shell	Multiplicity	Unrelaxed position	Relaxed position
1	12	1/2, 1/2, 0	0.4905, 0.4905, 0
2	6	0, 0, 1	0, 0, 0.9990
3	24	1/2, 1/2, 1	0.4988, 0.4988, 0.9985
4	12	1, 1, 0	0.9970, 0.9970, 0

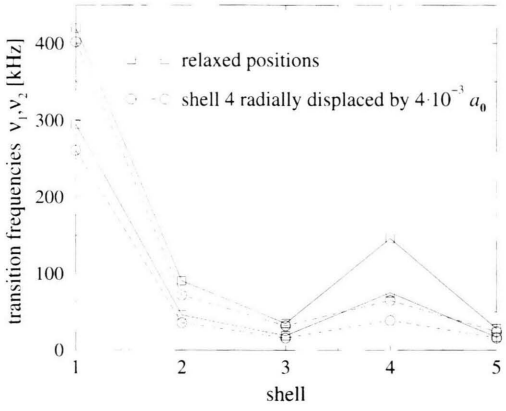

Fig. 2. Transition frequencies ν_2 (upper curves) and ν_1 around monovacancies in Al as calculated with a 124-atom supercell and the plane-wave pseudopotential method with subsequent reconstruction of the true valence wavefunctions. The core contribution has been neglected. The squares have been obtained with the relaxed positions; the circles result from an outward displacement of shell 4 by $4 \cdot 10^{-3}\, a_0$. The lines serve only to guide the eyes.

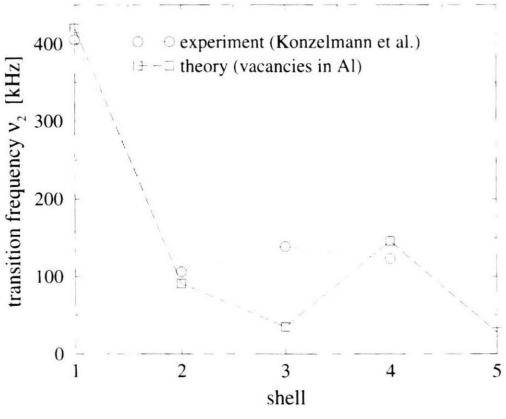

Fig. 3. *Circles:* Transition frequencies ν_2 observed after low-temperature electron irradiation, quenching, or cold-work of Al. *Squares:* Values computed for a monovacancy using a 124-atom supercell and the plane-wave pseudopotential method. The core polarization has been neglected.

Table 3. Experimental and theoretical values of η around a monovacancy in Al. The theoretical values were computed with a 124-atom supercell and the pseudopotential method.

Shell	1	2	3	4	5
η (theory)	0.59	0	0.24	0.14	0.40
η (experiment)	0.67–0.71	$\simeq 0$	0.24–0.41	0.11–0.41	–

The entry zero (0) means that η vanishes by symmetry. For the first shell the experimental and theoretical values of the transition frequencies (see Fig. 3) and of η are in good agreement. This leads to the conclusion that the experimental lines at 405 and 310 kHz are due to the nearest neighbours of monovacancies. The fact that this pair of lines is observed not only after electron irradiation and cold-work but also after quenching from high temperatures supports this interpretation.

Ferreira and Frota-Pessôa have calculated the efg acting on the nearest neighbours of a monovacancy in Al using the real-space linear-muffin-tin-orbital approach [59]. Neglecting lattice relaxation (cf. Sect. 1.2) they obtained $\nu_2 = 350$ kHz and $\eta = 0.57$. According to our computations the lattice relaxation causes the efg at the nearest-neighbour site to increase by a factor $\simeq 1.15$. Hence the result of Ferreira and Frota-Pessôa, as far as it goes, is in good agreement with ours.

For the shells 2, 3 and 4 a final statement cannot be made at present time. On the one hand, the computed values are subject to the uncertainties due to the finite size effects discussed. On the other hand, the assignment of Konzelmann, although similar to that of Minier [12], should not be considered definitive.

The best check of the reliability of the methods described in Sect. 1 is to compute the efg around substitutional foreign atoms and to compare them with experiments on dilute alloys. In this case the assignment of the measured transition frequencies to distinct shells is much easier since one can be sure that all lines in the NQDOR spectrum are due to only one atomic defect, namely the substitutional foreign atom. Using a small supercell of 16 atoms only, FLAPW calculations have been carried out on substitutional vanadium and iron atoms in Al. Since for this supercell size the second shell already lies on the supercell surface, the only atomic positions that could be relaxed were those in the first shells surrounding the foreign atoms. For comparison, an FLAPW calculation with a supercell of 15 atoms has been performed on a monovacancy, too. The results of these two calculations are given in Tables 4 and 5.

As may be seen from Table 4, the nearest-neighbour relaxations are about the same for vanadium and for monovacancies but are substantially larger for iron. The comparison with Table 2 shows that the small supercell calculation underestimates the relaxations, but only moderately so.

Table 5 compares the calculated transition frequencies ν_2 and ν_1 and the corresponding η with the exper-

Table 4. Relaxation of the first shell around the substitutional foreign atoms V and Fe, and a monovacancy in Al as computed for 16-(15-)atom supercells by the FLAPW method.

Unrelaxed position	Relaxed positions		
	V	Fe	monovacancy
1/2, 1/2, 0	0.492, 0.492, 0	0.486, 0.486, 0	0.492, 0.492, 0

Table 5. Quadrupolar transition frequencies of the first shell surrounding the substitutional foreign atoms V and Fe, and the monovacancy in Al as computed for 16-(15-)atom supercells by the FLAPW method. The core contribution has been calculated with the "one-shot approximation". In the respective third lines the experimental value for η and the theoretical value for V_{zz} have been used.

		η	ν_2 [kHz]	ν_1 [kHz]	$V_{zz}^{\text{core}}/V_{zz}^{\text{val+lat}}$
V	theory	0.2	1220	650	+0.08
	experiment [11]	0.12	1250	635	
	theory with experimental η	0.12	1230	620	
Fe	theory	0.7	470	360	+0.30
	experiment [11]	0.57	500	345	
	theory with experimental η	0.57	480	330	
mono-vacancy	theory	0.9	390	380	−0.15
	experiment [12, 15]	0.69	405	310	
	theory with experimental η	0.69	415	315	

imental values [11, 12, 15]. The third line in each entry gives the frequencies ν_2 and ν_1 if they are calculated by combining the computed efg with the experimentally determined asymmetry. Considering the small supercell size used, the agreement between the experimental and theoretical frequencies may be called acceptable. By contrast, the calculated η values are much too large; so one should always use experimental asymmetries if small supercells are employed.

Table 5 also gives the core contributions (from 1s, 2s, and 2p electrons) to the large component (V_{zz}) of the efg acting on the nearest-neighbour nuclei as calculated by the "one-shot approximation" of Sect. 1.3. In order to test the reliability of this approximation for substitutional iron the computation of the aspherical core-electron density was included in the self-consistency cycle of the FLAPW method. This computation yielded values for ν_2 and η very similar to those of the "one-shot approximation", namely $\nu_2 = 460$ MHz and $\eta = 0.7$. Hence, the reaction of the valence electrons to the asphericity of the core-electron density is completely negligible. Figure 4 shows indeed that the $l = 2$, $m = 0$ component of the core-electron density,

$$n_{20}^{c}(r) = \int n_c(\boldsymbol{r})\, Y_{20}^{*}(\hat{r})\, d\Omega\,, \tag{29}$$

which dominates the core contribution to the efg, see (26), is small compared with the corresponding component of the valence-electron density. Because of the weighting of the core-electron density in (26) by the factor r^{-3}, the core contribution to the efg is nevertheless important but apparently handled well enough by the the "one-shot approximation". Furthermore, the additional contribution of the 2p electrons of Al of the efg acting on the nearest-neighbour site of a substitutional iron atom has been considered using the local-orbital method implemented in the new FLAPW code WIEN95 [56]. This calculation gave $\nu_2 = 440$ kHz and $\eta = 0.9$. With the "one-shot approximation" we obtain $\nu_2 = 480$ kHz and $\eta = 0.8$ if only the contributions of the 2p core electrons and of the valence electrons are taken into account.

The efg surrounding a $\langle 100 \rangle$ *dumb-bell* – the stable self-interstitial configuration in fcc metals – have been calculated for a 65-atom supercell using the FLAPW method. Here shell 4 lies on the surface of the supercell. The relaxed atomic positions up to shell 3 are shown in Table 6. Table 7 gives the transition frequencies computed using these positions as well as the contribution of the core electrons (1s, 2s, and 2p) to the efg as determined by the "one-shot approximation". The fact that this contribution comes out rather

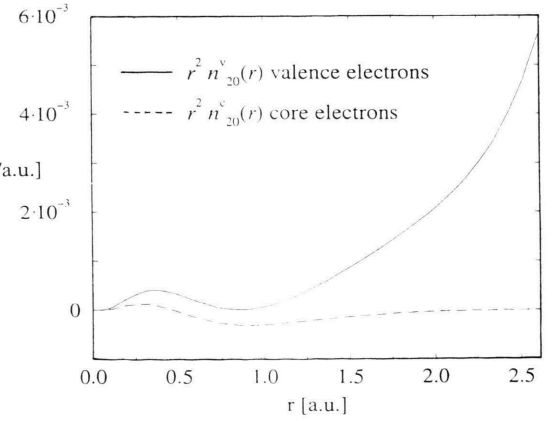

Fig. 4. $l = 2$, $m = 0$ component of the valence and core-electron density times r^2 at the nearest-neighbour atoms of substitutional iron in Al (1 a.u. = 0.529 Å).

Table 6. Positions of the nuclei surrounding a ⟨100⟩ dumb-bell in Al in units of a_0 as computed with a 65-atom supercell and the FLAPW method.

Shell	Multiplicity	Unrelaxed positions	Relaxed positions
0 (dumb-bell atoms)	2	0, 0, 0	0, 0, 0.292
1′	4	1/2, 1/2, 0	0.470, 0.470, 0
1″	8	0, 1/2, 1/2	0, 0.564, 0.534
2′	2	0, 0, 1	0, 0, 0.994
2″	4	1, 0, 0	1.004, 0, 0
3′	8	1/2, 1/2, 1	0.503, 0.503, 1.012
3″	16	1, 1/2, 1/2	1.003, 0.507, 0.494

Table 7. Transition frequencies ν_2 and ν_1, asymmetry η, and core contribution to the efg for a ⟨100⟩ dumb-bell in Al as computed with a 65-atom supercell and the FLAPW method.

Shell	Multiplicity	η	ν_2 [kHz]	ν_1 [kHz]	$V_{zz}^{\text{core}}/V_{zz}^{\text{val+lat}}$
0	2	0	560	280	−0.24
1′	4	0.4	460	280	−0.05
1″	8	0.2	1760	920	+0.04
2′	2	0	300	150	+0.17
2″	4	≃1	210	200	−0.11
3′	8	0.8	350	300	+0.08
3″	16	0.2	500	270	+0.09

large for the efg acting on the dumb-bell atoms has to be considered with caution for two reasons:

1. For small distances from the nucleus the asphericity of the core-electron density is not small compared with the asphericity of the valence-electron density, hence it should be included in the self consistency cycle.
2. Since the two "dumb-bell atoms" are separated by about $0.6\,a_0$ only, their 2p orbitals overlap. This means that these orbitals should not be treated as "core states" in the sense of the general theory of Sect. 1, as was done so far.

Up to now, none of the calculated dumb-bell frequencies have been observed experimentally. This may have several reasons. There will almost certainly be an intensity problem because of the small multiplicity of some of the subshells, particularly so for shell 0 and subshell 2′ which have multiplicity 2. The smaller frequencies may overlap not only with other self-interstitial frequencies but also with vacancy frequencies, since self-interstitials are always generated together with a comparable density of vacancies. When searching for the dumb-bell lines it should be kept in mind that those associated with the 0th shell are uncertain because of the problems discussed above, and that those of the higher shells may be affected by finite-size effects.

2.2.2 Results on Cu

The supercell calculations reported in this subsection have all been performed by means of the FLAPW method. The transition frequencies given pertain to the isotope ^{63}Cu; those of ^{65}Cu are 7.3% lower.

Table 8 gives the relaxed positions of the atoms in the first shell around various substitutional foreign atoms as calculated with 16-atom supercells. The relaxations of the nearest neighbours of a monovacancy as given by the corresponding calculation (15-atom supercell) are negligibly small. The transition frequencies in shell 1 computed from these results are listed in Table 9 using the experimentally determined lattice parameters or (in some cases) the smaller values following from ab-initio LDA calculations. The entries in the last two columns are those observed transition

Table 8. Positions of the nuclei in the first shell surrounding substitutional Be, Ni, Pd, and Pt atoms in Cu in units of a_0 as computed with a 16-atom supercell and the FLAPW method.

Unrelaxed position	Relaxed positions			
	Be	Ni	Pd	Pt
1/2, 1/2, 0	0.495, 0.495, 0	0.498, 0.498, 0	0.507, 0.507, 0	0.509, 0.509, 0

Table 9. Transition frequency ν_q (for ^{63}Cu), asymmetry η, and core contribution to the efg for the first shell surrounding substitutional foreign atoms and a monovacancy in Cu as computed with a 16-(15-)atom supercell and the FLAPW method.

	Ab-initio a_0	Experimental a_0		$V_{zz}^{\text{core}}/V_{zz}^{\text{val+lat}}$	Experiment	
	ν_q [MHz]	ν_q [MHz]	η		ν_q [MHz]	η
Be	2.8	2.4	0.2	−0.03	2.0	–
Ni	–	1.3	0.5	+0.25	1.1	0.2
Pd	3.6	3.1	0.3	−0.06	3.2	0.2
Pt	–	4.3	0.5	−0.09	4.7	–
mono-vacancy	3.6	3.0	0.1	−0.19	3.4	–

frequencies [3, 5, 15] that are closest to the calculated ones and experimental values for asymmetry, which have been determined by NMR [62]. Furthermore, Table 9 contains the calculated asymmetries and the ratios of the core contributions (1s–3p electrons) to the sum of the valence-electron and lattice contributions.

Considering the smallness of the supercells used, the agreement between the measured and the computed frequencies is quite good, particularly so if for the latter the experimental a_0 are used. However, to some extent this agreement may be fortuitous. The calculated asymmetries at the nearest-neighbour nuclei of substitutional Ni or Pd atoms are – as for the substitutional foreign atoms in Al (see Table 5) – too large compared with the experimental values. A further error of limited but unknown magnitude comes in because of the uncertainty in the nuclear quadrupole moments of ^{63}Cu and ^{65}Cu discussed in the Introduction. This error is systematic, however, and may be corrected by adjustment if a large enough body of accurate computations and reliable experimental data becomes available.

As Table 9 shows, the effect of the core electrons on the efg can be quite large. This has been studied in more detail for the case of substitutional Ni. Although here the "one-shot approximation" gave a rather large core-electron contribution, the inclusion of the aspherical core-electron density in the self-consistency cycle did not change the V_{zz} and η values. As Fig. 5 shows, the (2,0) component of the core-electron density is indeed much smaller than that of the valence-electron density. This demonstrates that in the present case it was justified to neglect the influence of the aspherical core-electron density. In addition, the so-called local-orbital approach [56] was applied to the 3p electrons. This gave $\nu_q = 1.2$ MHz and $\eta = 0.6$, in good agreement with the result $\nu_q = 1.2$ MHz and $\eta = 0.5$ of the simpler "one-shot approximation" treatment of the 3p electrons.

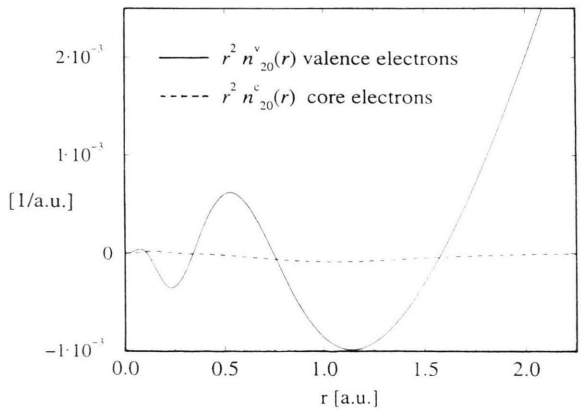

Fig. 5. $l = 2$, $m = 0$ component of the valence and core-electron density times r^2 at the nearest-neighbour atoms of substitutional Ni in Cu (1 a.u. = 0.529 Å).

For the monovacancy an additional calculation was performed with a 63-atom supercell. In this case shell 4 lies on the cell boundary, so that the atomic positions up to shell 3 may be relaxed. However, the forces acting on the shell-3 atoms come out so small that their relaxation could be neglected. The relaxed positions for the first two shells are given in Table 10. Note that the displacements at the next-nearest neighbour atoms, while still small ($3.6 \cdot 10^{-3}\, a_0$), are much larger than those of the nearest neighbours of the vacant site. This may mean that in order to obtain the displacement field around a monovacancy in copper accurately, we may have to use larger supercells.

The quadrupolar transition frequencies of the nuclei in the first three shells surrounding a monovacancy are listed in Table 11 together with the asymmetries and with the core contributions to the efg as calculated by the "one-shot approximation". For the first shell the transition frequencies obtained with the 15-atom or the 63-atom supercell are in reasonable agreement; they differ only by approximately 10%. The computed asymmetry of the efg tensor acting on the nuclei in the first shell is substantially smaller than in the case of Al.

Table 10. Positions of the nuclei surrounding monovacancies in Cu in units of a_0 as computed with a 63-atom supercell and the FLAPW method.

Shell	Multiplicity	Unrelaxed positions	Relaxed positions
1	12	1/2, 1/2, 0	0.4992, 0.4992, 0
2	6	0, 0, 1	0, 0, 0.9964
3	24	1/2, 1/2, 1	0.500, 0.500, 1.000

Table 11. Transition frequency ν_q (for ^{63}Cu), asymmetry η, and core contribution to the efg for a monovacancy in Cu as computed with a 63-atom supercell and the FLAPW method.

Shell	Multiplicity	η	ν_q [MHz]	$V_{zz}^{\text{core}}/V_{zz}^{\text{val+lat}}$
1	12	0.2	3.3	−0.16
2	6	0	0.4	+0.63
3	24	0.0	0.5	+0.11

The two calculations of the quadrupolar transition frequencies ν_q associated with monovacancies in Cu [59, 60] disregard the lattice relaxation. This may not be a too serious approximation in the present case but is in general not permitted. In their real-space linear-muffin-tin-orbital calculation Ferreira and Frota-Pessôa [59] neglected, in addition, the core contribution to the efg. The fact that they obtained $\eta \simeq 1$, i.e. a much higher asymmetry than predicted by the FLAPW method, may point towards a basis weakness of the linear-muffin-tin-orbital method in combination with the ASA for the calculation of efg tensors in solids. Correcting for this high η value reduces the transition frequency $\nu_q = 4.3$ MHz computed by Ferreira and Frota-Pessôa [59] to about 3.8 MHz. If we apply further the correction for the neglected core contribution as given in Table 11, we obtain finally $\nu_q = 3.2$ MHz, which is in satisfactory agreement with the FLAPW calculation for the 63-atom supercell.

The calculation of Drittler et al. [60], using the KKR-GF method (see Sect. 1.2), give $\nu_q = 5.6$ MHz if we replace the quadrupole moment $Q(^{63}\text{Cu}) = 160 \cdot 10^{-31}\ \text{m}^2$ by the value $220 \cdot 10^{-31}\ \text{m}^2$ used through this paper (cf. Introduction).

Transition frequencies that might be attributed to the first three shells surrounding monovacancies in Cu have been found after low-temperature electron and proton irradiation [3, 5, 13, 15] as well as after cold-work [3, 15]. However, none of these lines have been observed after quenching of liquid or solid Cu [15, 16], i.e. under conditions at which a fairly large concentration of monovacancies should be frozen in. The present situation must therefore be considered as inconclusive.

The results of a 65-atom-supercell calculation of the relaxed atom positions and of the efg in the neighbourhood of ⟨100⟩ dumb-bells are shown in Tables 12 and 13. It is remarkable that the positions of the nuclei are in excellent agreement with the positions predicted by an early calculation [61] based on a rather sophisticated model potential. In particular, the separation between the two dumb-bell atoms was predicted to be $0.60\,a_0$, which agrees well with the value $0.58\,a_0$ in Table 12. The core contribution to the efg acting on the two "dumb-bell nuclei" (zeroth shell) should – for the same reasons as in the case of Al – be considered with some caution.

The comparison with the experimentally observed lines [3, 5, 13] encounters difficulties analogous to those discussed in Sect. 2.2.1. Moreover, of the shells with high multiplicity, the predicted ν_q for subshell 1″ lies outside the range covered by the experiments (20 kHz to 6 MHz in [3]), whereas those of the subshells 3′ and 3″ must be considered as very uncertain because of finite-cellsize effects. It is therefore too early to say to what extent contact has been made between experiment and theory. It is clearly necessary to increase the cell size in order to obtain reliable estimates for the field gradient in subshell 3′ and in particular in subshell 3″ and to extend the search for transition frequencies of subshell 1″ to higher frequencies.

Table 12. Positions of the nuclei in the neighbourhood of a ⟨100⟩ dumb-bell in Cu up to shell 3 in units of a_0 as computed with a 65-atom supercell and the FLAPW method.

Shell	Multiplicity	Unrelaxed positions	Relaxed positions
0 (dumb-bell atoms)	2	0, 0, 0	0, 0, 0.289
1′	4	1/2, 1/2, 0	0.476, 0.476, 0
1″	8	0, 1/2, 1/2	0, 0.565, 0.530
2′	2	0, 0, 1	0, 0, 0.997
2″	4	1, 0, 0	1.007, 0, 0
3′	8	1/2, 1/2, 1	0.506, 0.506, 1.005
3″	16	1, 1/2, 1/2	1.004, 0.508, 0.494

Table 13. Transition frequency ν_q (for ^{63}Cu), asymmetry η, and core contribution to the efg for a ⟨100⟩ dumb-bell in Cu as computed with a 65-atom supercell and the FLAPW method.

Shell	Multiplicity	η	ν_q [MHz]	$V_{zz}^{\text{core}}/V_{zz}^{\text{val+lat}}$
0	2	0	0.5	−1.40
1′	4	0.9	1.3	−0.15
1″	8	0.3	6.9	+0.09
2′	2	0	1.7	−0.17
2″	4	0.5	1.3	−0.20
3′	8	0.7	0.5	−0.29
3″	16	0.3	2.9	+0.15

3. Summary

In combination with the supercell technique the FLAPW method as well as the plane-wave pseudopotential method with subsequent reconstruction of the correct valence-electron density have proved to be powerful tools for the ab-initio calculation of electric field gradients in the neighbourhood of atomic defects in metals. This is demonstrated by the agreement be-

tween experiment and theory for the quadrupolar transition frequencies of the nearest-neigbour nuclei of several substitutional foreign atoms in Al and Cu. The investigation also showed that the influence of the core electrons on the electric field gradient can be very large and should therefore not be neglected. In Al the calculated transition frequencies of the nuclei in shell 1 around a monovacancy and the largest experimentally observed frequencies are in excellent agreement. This, together with the fact that these lines are also present in the NQDOR spectrum after quenching Al samples from high temperatures, leads to the conclusion that the lines originate from the nearest-neighbour nuclei of monovacancies. The assignment of the other experimentally observed lines to distinct shells around specific atomic defects is not possible at present. In Cu there seems to be good agreement between the calculated transition frequency of the nearest-neighbour nuclei around a monovacancy and the highest transition frequency observed in the NQDOR spectrum after electron and proton irradiation as well as after cold-work. The tentative attribution of this transition to the nearest neighbours of monovacancies is in conflict with the fact that the line has not been observed after quenching Cu from high temperatures, however. The definitive assignment of the NQDOR lines observed in Al and Cu after different pretreatments to distinct shells around specific atomic defects requires further experimental and theoretical investigations.

Acknowledgements

The authors would like to express their thanks to Dipl. Phys. B. Meyer, Dipl. Phys. U. Breier and Dr. C. Elsässer for their help in performing the pseudopotential calculations and in using the reconstruction program. Without their help these computation could not have been performed. They are also indebted to Dipl. Phys. H. G. Krimmel for the implementation of the force formula of Soler and Williams in the FLAPW code. Further, the authors are grateful to Dipl. Phys. K. Konzelmann for detailed discussions of his NQDOR measurements and to Prof. K. Schwarz and Dr. P. Blaha (Vienna) for making the FLAPW codes WIEN 93 and WIEN 95 available to us. In the final stage of this work one of the authors (A. S.) held a Gledden Senior Visiting Fellowship at the University of Western Australia.

[1] N. Bloembergen, Nuclear Resonance in Crystals, in: Defects in Crystalline Solids (Report of the Conference held at the H. H. Wills Laboratory, University of Bristol, July 1954), The Physical Society, London 1955, p. 1.
[2] A. G. Redfield, Phys. Rev. **130,** 589 (1963).
[3] M. Notter, K. Konzelmann, G. Majer, and A. Seeger, Z. Naturforsch. **49a,** 47 (1994).
[4] M. Blanz, M. Hampele, G. Majer, M. Notter, and A. Seeger, in: Congress Ampere in Magnetic Resonance and Related Phenomena (M. Mehring, J. Schütz, and H. Wolf, eds.), Springer, Berlin 1990, p. 38.
[5] M. Minier and C. Minier, Phys. Rev. B **22,** 21 (1980).
[6] M. Minier, Phys. Rev. **182,** 437 (1969).
[7] C. Berthier and M. Minier, Phys. Rev. B **7,** 1854 (1973).
[8] C. Berthier and M. Minier, J. Phys. F: Metal Phys. **3,** 1169 (1973).
[9] C. Berthier and M. Minier, J. Phys. F: Metal Phys. **3,** 1268 (1973).
[10] M. Minier and S. Ho Dung, J. Phys. F: Metal Phys. **7,** 503 (1977).
[11] C. Berthier and M. Minier, J. Phys. F: Metal Phys. **7,** 515 (1977).
[12] M. Minier, R. Andreani, and C. Minier, Phys. Rev. B **18,** 102 (1978).
[13] C. Minier, M. Minier, and R. Andreani, Phys. Rev. B **22,** 28 (1980).
[14] M. Notter and A. Seeger, NQI Newsletter **1** (3), 16 (1994).
[15] K. Konzelmann, oral presentation at XIIIth Intern. Symp. Nuclear Quadrupole Interactions, Providence, Rhode Island, 1995.
[16] K. Konzelmann, G. Majer, M. Notter, and A. Seeger, Phil. Mag. Letters **70,** 23 (1994).
[17] D. Sundholm and J. Olsen, Phys. Rev. Letters **68,** 927 (1992).
[18] P. Pyykkö and J. Li, Nuclear Quadrupole Moments, Report HUKI 1-92, Helsinki (1992), (ISSN 0784-0365).
[19] T. P. Das and E. L. Hahn, in: Solid State Physics, Supplement 1, (F. Seitz and D. Turnbull, eds.), Academic Press, New York 1958, p. 1.
[20] G. S. Harbison, A. Slokenbergs, and T.M. Barbara, J. Chem. Phys. **90,** 5292 (1989).
[21] M. Born and J. R. Oppenheimer, Ann. Physik **84,** 457 (1927).
[22] R. E. Peierls, Quantum Theory of Solids, Clarendon Press, Oxford 1955.
[23] P. Hohenberg and W. Kohn, Phys. Rev. **136,** B 864 (1964).
[24] W. Kohn and L. J. Sham, Phys. Rev. **140,** A 1133 (1965).
[25] D. M. Ceperley and B. J. Alder, Phys. Rev. Letters **45,** 566 (1980).
[26] J. P. Perdew, J. A. Chevary, S. H. Vosko, K. A. Jackson, M. R. Pederson, D. J. Singh, and C. Fiolhais, Phys. Rev. B **46,** 6671 (1992).
[27] A. Garcia, C. Elsässer, J. Zhu, and S. G. Louie, Phys. Rev. B **46,** 9829 (1992).

[28] F. Bloch, Z. Physik **52,** 555 (1929).
[29] P. Blaha, K. Schwarz, P. Sorantin, and S. B. Trickey, Comp. Phys. Commun. **59,** 399 (1990).
[30] P. Blaha, K. Schwarz, and R. Augustyn, WIEN 93 (Improved and updated Unix version of the original copyright WIEN-Code of reference [29]), Technical University of Vienna, Wien 1993.
[31] W. E. Pickett, Computer Phys. Rep. **9,** 115 (1989).
[32] H. Hellmann, J. Chem. Phys. **3,** 61 (1935).
[33] H. Hellmann and W. Kassatotschkin, J. Chem. Phys. **4,** 324 (1936).
[34] P. Gombás, Pseudopotentiale, Springer-Verlag, New York 1967.
[35] E. Fues and H. Statz. Z. Naturforsch. **7a,** 2 (1952).
[36] V. Heine and I. Abarenkov, Phil. Mag. **9,** 451 (1964).
[37] D. R. Hamann, M. Schlüter, and C. Chiang, Phys. Rev. Letters **43,** 1494 (1979).
[38] B. Meyer, Diplomarbeit, Universität Stuttgart, Stuttgart 1994.
[39] B. Meyer, K. Hummler, C. Elsässer, and M. Fähnle, J. Phys.: Condens. Matter, **7,** 9201 (1995).
[40] H. Hellmann, Einführung in die Quantenchemie, Deuticke, Leipzig 1937.
[41] J. M. Soler and A. R. Williams, Phys. Rev. B **40,** 1560 (1989).
[42] H. G. Krimmel, J. Ehmann, C. Elsässer, M. Fähnle, and J. M. Soler, Phys. Rev. B **50,** 8846 (1994).
[43] M. Fähnle, C. Elsässer, and H. G. Krimmel, Phys. Stat. Sol. (b) **191,** 9 (1995).
[44] P. H. Dederichs and R. Zeller, in: Festkörperprobleme, vol. 21, (J. Treusch, ed.), Vieweg, Braunschweig 1981, p. 243.
[45] J. Korringa, Physica **13,** 392 (1947).
[46] W. Kohn and N. Rostoker, Phys. Rev. **94,** 1111 (1954).
[47] P. H. Dederichs, T. Hoshino, B. Drittler, K. Abraham, and R. Zeller, Physica B **172,** 203 (1991).
[48] H. M. Petrilli and S. Frota-Pessôa, J. Phys.: Condens. Matter **2,** 135 (1990).
[49] O. K. Andersen, Phys. Rev. B **12,** 3060 (1975).
[50] T. P. Das and P. C. Schmidt, Z. Naturforsch. **41a,** 47 (1986).
[51] S. Lauer, V. R. Marathe, and A. Trautwein, Phys. Rev. A **19,** 1852 (1979).
[52] R. M. Sternheimer, Z. Naturforsch. **41a,** 24 (1986).
[53] E. N. Kaufmann and R. J. Vianden, Rev. Mod. Phys. **51,** 161 (1979).
[54] M. H. Cohen and F. Reif, in: Solid State Physics, vol. 5, (F. Seitz and D. Thurnbull, eds.), Academic Press, New York 1957, p. 321.
[55] D. Singh, Phys. Rev. B **43,** 6388 (1991).
[56] P. Blaha, K. Schwarz, P. Dufek, and R. Augustyn, WIEN 93 (Improved and updated Unix version of the original copyrighted WIEN-Code of reference [29]), Technical University of Vienna, Wien 1995.
[57] A. Seeger, P. Schiller, and H. Kronmüller, Phil. Mag. **5,** 853 (1960).
[58] P. Blaha, K. Schwarz, and P. H. Dederichs, Phys. Rev. B **37,** 2792 (1988).
[59] S. Ferreira and S. Frota-Pessôa, Phys. Rev. B **51,** 2045 (1995).
[60] B. Drittler, M. Weinert, R. Zeller, and P. H. Dederichs, Phys. Rev. B **42,** 9336 (1990).
[61] A. Seeger, E. Mann, and R. von Jan, J. Phys. Chem. Solids **23,** 639 (1962).
[62] R. Nevald and G. Petersen, J. Phys. F: Metal Phys. **5,** 1778 (1975).